Journal of Catalysis 260 (2008) 295–304

Contents lists available at ScienceDirect

Journal of Catalysis

www.elsevier.com/locate/jcat

Effective silica supported Sb–V mixed oxide catalyst for selective oxidation of methanol to formaldehyde

Haidong Zhang, Zhimin Liu, Zhaochi Feng, Can Li *

State Key Laboratory of Catalysis, Dalian Institute of Chemical Physics, Chinese Academy of Sciences, Dalian 116023, China

ARTICLE INFO

Article history:
Received 4 July 2008
Revised 23 September 2008
Accepted 24 September 2008
Available online 23 October 2008

Keywords:
Sb–V mixed oxide
Selective oxidation
Methanol
Formaldehyde

ABSTRACT

Silica supported Sb–V mixed oxide catalysts ($VSbO_x/SiO_2$) were prepared and evaluated in methanol selective oxidation. One-pass yield of formaldehyde at 91% was obtained on one $VSbO_x/SiO_2$ catalyst. The active phase of $VSbO_x/SiO_2$ catalysts is found to be Sb–V mixed oxide, in which isolated VO_x species can be stabilized. The relative amount of monomeric VO_x species in $VSbO_x/SiO_2$ catalyst is higher than pure supported VO_x catalyst. On $VSbO_x/SiO_2$ catalyst, the deep oxidation of intermediates is greatly depressed because the formation of adsorbed acyl species, which leads to CO_x, is not favored. The average oxidation state of the vanadium in $VSbO_x/SiO_2$ catalysts increases with decreasing Sb/V ratio. Higher oxidation state of the vanadium in $VSbO_x/SiO_2$ catalysts is found to be relevant to higher activity while V^{4+} species are more selective to formaldehyde. Sb–V mixed oxide catalyst provides a possibility to adjust the production distribution in methanol selective oxidation by changing Sb/V ratio.

1. Introduction

Selective oxidation of methanol to formaldehyde, which is an important building block for some complex chemicals, is one of the dominant oxidation processes in industry [1]. The current industrialized processes for this transform from methanol to formaldehyde are based on silver catalysts and iron molybdate catalysts. Recently, supported vanadia catalysts were found to be promising catalysts for this reaction [2–5]. Vanadia catalysts have been found to be structurally sensitive for this reaction [2,6–9]. The active species of supported vanadia catalysts are proposed to be isolated tetrahedrally coordinated VO_4 species [2] or adjacent VO_4 units [8] with V=O bands as remarkable characteristic. The polymerized VO_x species with V–O–V bonds are suggested not to be involved in methanol selective oxidation but usually relevant to deep oxidation [8]. The formation of aggregated or crystalline vanadia species results in the drops in both methanol conversion and formaldehyde selectivity [5,7]. Kim and Wachs found that, in the methanol oxidation catalyzed by V_2O_5/Al_2O_3 catalysts, the crystalline V_2O_5 nanoparticles above monolayer coverage were relatively inactive and served only to decrease the number of exposed catalytic active surface vanadia sites by covering them [3].

However, the aggregation of highly isolated vanadia species under reaction conditions is always a puzzle. Consequently, high specific area materials like MCM-41 [10], MCM-48 [7] and SBA-15 [5,11,12] were employed as supports to decrease the surface concentration of vanadia species and then promote the well dispersion of vanadia species. In addition, some novel grafting methods were adopted together with the high specific area supports in order to benefit the isolation of vanadia species [5,7]. As another option within the efforts to develop active catalyst for the selective oxidation of methanol, mixed oxides have been of great interest because of the opportunity to adjust the variation in active sites [9,13,14].

Sb–V mixed oxide catalysts have been widely used for selective oxidation of hydrocarbons [15,16]. Benvenutti and Gaushikem found that the deep oxidation of methanol or formaldehyde can be depressed with the presence of antimony species [17]. Additionally, Spengler et al. found that the aggregation of vanadia species can be interrupted in Sb–V mixed oxide by means of the formation of V–O–Sb–O–V species [18]. In our previous work, we found that V=O in common with Sb–O–V sites prevail in the Sb–V mixed oxides dispersed on MSU-2 [19] or amorphous silica [20] and the speciation of supported Sb–V mixed oxides can be tuned by changing Sb/V ratio. Furthermore, the surface acidity of supported Sb–V mixed oxide catalysts is adjustable due to the interaction of antimony and vanadium atoms [14]. It has been found that, in methanol selective oxidation, the production of formaldehyde needs bi-functional catalysts with acid–base character [21–23]. It can be expected that Sb–V mixed oxide catalysts may show promising activity and selectivity in methanol selective oxidation.

In this work, we prepared and investigated silica supported Sb–V mixed oxide catalysts ($VSbO_x/SiO_2$) in the selective oxidation of methanol with O_2 as oxidant. As the comparison of $VSbO_x/SiO_2$ catalysts, silica supported vanadia catalysts (VO_x/SiO_2) with corresponding loading of vanadia to that for the $VSbO_x/SiO_2$ catalysts were prepared and investigated under same reaction conditions. In

* Corresponding author. Fax: +86 411 84694447.
E-mail address: canli@dicp.ac.cn (C. Li).

0021-9517/$ – see front matter
doi:10.1016/j.jcat.2008.09.019

$VSbO_x/SiO_2$ catalysts, the framework of VO_x species is interrupted by the incorporation of Sb atoms and isolated VO_x species can be stabilized in the framework of Sb–V mixed oxide. In the methanol selective oxidation with O_2 as oxidant, $VSbO_x/SiO_2$ catalysts exhibit very stable catalytic performance with high selectivity to formaldehyde but low selectivity to CO_x. One-pass yield of formaldehyde at 91% can be achieved on $VSbO_x/SiO_2$ catalyst. *In situ* diffuse reflectance infrared Fourier transform spectroscopy (DRIFTS) studies exhibit that the $VSbO_x/SiO_2$ catalysts can greatly depress the overoxidation to form CO_x.

2. Experimental

2.1. Catalyst preparation

$VSbO_x/SiO_2$ catalysts were prepared by a two-step incipient wetness impregnation method. Silica (Qingdao Mandarin Chemical Group, China) was firstly impregnated with $SbCl_5$ (Acros, 99.5%)–ethanol solution [24], and then dried at room temperature. Antimony precursors can be well dispersed on silica surface after this impregnation step [17,18,24,25]. The dried solid product was then impregnated for the second time with aqueous solution of NH_4VO_3 (Shanghai Chemical Reagent Co., Ltd.) [20] and then dried at room temperature. Aqueous ammonia solution was used to adjust the pH value of the final impregnates to 8–9. All solid products were then dried at 120 °C and then calcined in air at 700 °C for 4 h to obtain $VSbO_x/SiO_2$ catalysts.

VO_x/SiO_2 catalysts were prepared by the incipient wetness impregnation of silica with aqueous solution of NH_4VO_3. A 20 wt% Sb_2O_5/SiO_2 catalyst (counted as Sb_2O_5) was prepared by incipient wetness impregnation of silica with $SbCl_5$–ethanol solution followed by an adjustment of pH value of the impregnate to 8–9 with aqueous ammonia. The procedures of the drying and calcination for Sb_2O_5/SiO_2 catalyst and VO_x/SiO_2 catalysts are same as that for $VSbO_x/SiO_2$ catalysts. The V_2O_5 loading for each VO_x/SiO_2 catalyst varies from 11.2 wt% to 5.6 wt% and then to 2.24 wt%.

The SbO_x concentrations of all $VSbO_x/SiO_2$ catalysts are counted as their weight loading of Sb_2O_5 and keep to 20 wt%. The V_2O_5 loadings of $VSbO_x/SiO_2$ catalysts increase from 2.24 wt% to 5.6 wt% and then to 11.2 wt%. Six concise denotations are used to mark $VSbO_x/SiO_2$ and VO_x/SiO_2 catalysts. $VSbO_x/SiO_2$ catalysts are labeled as 11.2V–Sb, 5.6V–Sb and 2.24V–Sb. VO_x/SiO_2 catalysts are labeled as 11.2V, 5.6V and 2.24V. The premix number in each denotation corresponds with the weight loading of VO_x (counted as V_2O_5) for this catalyst. Correspondingly, the expected Sb/V atom ratio for $VSbO_x/SiO_2$ catalysts decreases from 5/1 (20 wt% Sb_2O_5, 2.24 wt% V_2O_5) to 2/1 (20 wt% Sb_2O_5, 5.6 wt% V_2O_5) and then to 1/1 (20 wt% Sb_2O_5, 11.2 wt% V_2O_5).

Sb_2O_5 was prepared by the hydrolysis of $SbCl_5$ and the calcinations of corresponding precipitates at 650 °C. Sb_2O_4 was prepared by the calcination of Sb_2O_3 (Shanghai Chemical Reagent Co., Ltd.) at 750 °C for 36 h [24,25]. V_2O_5 was used as received from Shanghai Chemical Reagent Co., Ltd.

2.2. Selective oxidation of methanol

Methanol selective oxidation tests were executed in a quartz tubular reactor using O_2 as oxidant. The flow rates of O_2 and He were separately controlled by two mass flow controllers while the mass flow rate of methanol vapor was controlled by passing a mixture of He and O_2 through a temperature-controlled saturator to produce a feed mixture of O_2/methanol/He in the molar ratio 1/1/21. In each test, 0.1 g catalyst was tested and the flow rate of gas-phase reaction mixture was 0.134 mol (STY) h^{-1}.

A gas chromatograph (Agilent 6890N) equipped with a ten-channel injection valve was employed to do on-line analysis of products. All pipes and the injection valve were heated to 120 °C. A Porapak Q column connected to Flame Ionized Detector (FID) was used to separate oxygenates, e.g., methanol and formaldehyde. A carbon molecular sieve column connected to Thermal Conductivity Detector (TCD) was used to separate He, O_2, CO and CO_2. External standard method was employed to estimate methanol conversion and products selectivity, using the standard gases (Dalian Gas Co., Ltd.) of CO, CO_2, O_2 and dimethyl ether (DME) and the standard samples (Chinese center of standard materials, Beijing) of formaldehyde and methanol to establish standard curves. The main products detected in the effluent of the reactions catalyzed by either $VSbO_x/SiO_2$ catalysts or VO_x/SiO_2 catalysts were found to be formaldehyde and CO_x. The production of DME is much lower than that of formaldehyde or CO_x while the production of other oxygenates in addition to formaldehyde and DME is little. The reported methanol conversion and formaldehyde selectivity values were calculated using following equations:

$$\text{methanol conversion} = \frac{M_{\text{in}} - M_{\text{out}}}{M_{\text{in}}} \times 100\%,$$

$$\text{formaldehyde selectivity} = \frac{M_{\text{HCHO}}}{M_{\text{in}} - M_{\text{out}}} \times 100\%,$$

where M_{in} and M_{out} are the amount (mol) of the methanol feed in and remaining in the effluent; M_{HCHO} is the amount (mol) of the formaldehyde detected in the effluent. The reaction tests were carried out with carbon balance in the range between 90% and 100% and the carbon balance value is higher than 95% in most tests.

2.3. Catalyst characterizations

For all catalysts, the content of vanadium or antimony was determined using inductively coupled plasma-atomic emission spectrometry (ICP-AES) on a Varian Vista spectrometer.

X-ray diffraction (XRD) measurements were performed on a Rigaku D/max-2500/PC X-ray diffractometer with Cu$K\alpha$ radiation (50 kV, 250 mA) from 15° to 70° with the scan speed at 2°/min.

N_2 adsorption–desorption analysis was done at 77 K on a Micromeritics TriStar 3000 instrument. The specific areas were calculated following Brunauer–Emmett–Teller (BET) method and the data of pore diameter were evaluated by Barrett–Joiner–Halenda (BJH) method from desorption isotherm plots.

UV Raman spectra were recorded on a Jobin-Yvon T64000 Raman spectrograph using 325 nm line of a 25 mW He–Cd laser as the excitation source.

All Fourier transform infrared spectroscopy (FT-IR) spectra were obtained on a Thermo Nicolet NEXUS 470 apparatus with a mercury–cadmium–telluride (MCT) detector at a resolution of 4 cm^{-1}. For the measurement of surface acidity, samples were pressed into self-supporting wafers (ca. 15 mg/cm^2) and put into a heatable quartz IR cell with CaF_2 windows. The samples were pretreated at 500 °C for 1 h under vacuum prior to pyridine adsorption. Then, after a 20 min balance of pyridine container in an ice-water bath, the samples were exposed to pyridine gas for 10 min at room temperature. After this, the samples were evacuated at room temperature to remove the pyridine in gas phase and weakly adsorbed pyridine. The temperature-programmed desorption of adsorbed pyridine was carried out by stepwise heating of sample under vacuum. FT-IR spectra were recorded at different temperatures. Difference spectra were obtained by subtracting the background spectrum of the unloaded sample.

For the *in situ* DRIFTS measurements of the adsorbed methanol on catalyst surface, an *in situ* DRIFTS chamber (Spectra-Tech 0019-037E) with ZnSe windows was used. Samples were firstly pretreated in the chamber in a mixture of He and O_2 at 500 °C. After

the pretreatment, only Si–OH groups and the framework vibrations of silica support were observed in FT-IR spectra. The adsorption of methanol was carried out by dosing the samples, in a stream of N_2–O_2 mixture through a methanol-containing Pyrex saturator, for 5 min at room temperature. Then methanol was omitted in the stream to remove the methanol in gas phase. The chamber was then rapidly heated to 350 °C. The record of DRIFTS spectra started while the temperature reaches 350 °C.

X-ray photoelectron spectroscopy (XPS) measurements were performed on a Shimadzu-Karatos Analytical AMICUS equipment using Mg$K\alpha$ radiation (12 kV, 10 mA) as excitation source. The binding energies values were relatively corrected according to the C 1s signal at 284.6 eV.

Ultraviolet–visible diffuse reflectance spectroscopy (UV–vis DRS) spectra were recorded on a JASCO V-550 UV–vis spectrophotometer using a home made in situ quartz cell. Before the acquisition of spectra at room temperature, samples were pretreated in a mixture of N_2 and O_2 ($N_2/O_2 = 7/3$, total flow rate is 30 ml/min) at 500 °C for 2 h. Scans were performed from 200 to 700 nm at a speed at 10 nm/min.

Temperature-programmed reduction (H_2-TPR) measurements were performed in a temperature-programmed apparatus equipped with a quartz tube reactor and a TCD detector. Samples were firstly pretreated in a mixture of N_2 and O_2 ($N_2/O_2 = 7/3$, total flow 25 ml/min) at 600 °C for 0.5 h, followed by purging with N_2 at room temperature for 1 h. Then, a flow of H_2–Ar mixture (5% H_2) was introduced into the reactor and the reactor was heated from room temperature to 950 °C at a rate of 8 °C/min.

3. Results and discussion

3.1. Textural and chemical properties of catalysts

In Fig. 1a we can see that the silica support and all catalysts show narrow distributions of pore size. The pore sizes of both VO_x/SiO_2 catalysts and $VSbO_x/SiO_2$ catalysts become smaller with increasing loading of V_2O_5. This trend is also indicated by the pore diameter values given in Table 1. For SbO_x/SiO_2 catalysts, SbO_x species are well dispersed on silica surface and the pore size and specific area just exhibit little drop even the loading of Sb_2O_5 reaches 20 wt% [24]. The specific areas of either VO_x/SiO_2 catalysts or $VSbO_x/SiO_2$ catalysts also remarkably decrease with increasing loading of V_2O_5 but remain a certain value at 255 m^2/g (for VO_x/SiO_2 catalysts) or 118 m^2/g (for $VSbO_x/SiO_2$ catalysts) even the V_2O_5 loading reaches 11.2 wt%. Fig. 1b exhibits the N_2 adsorption–desorption isotherms of the silica, 5.6V and 5.6V–Sb catalysts. In Fig. 1b, we can see that the silica, 5.6V and 5.6V–Sb catalysts present representative type IV isotherms [26], with hysteresis loops typical of ordered mesoporous materials. The real Sb/V ratio values for $VSbO_x/SiO_2$ catalysts are 5.2, 2.1 and 1.0 according to the ICP-AES results shown in Table 1.

3.2. Speciation on $VSbO_x/SiO_2$ catalysts

3.2.1. XRD studies on $VSbO_x/SiO_2$ catalysts

Fig. 2 shows the XRD patterns of $VSbO_x/SiO_2$ catalysts, V_2O_5, Sb_2O_4 and Sb_2O_5. Sb–V mixed oxides have non-stoichiometric rutile type structure and the nature of Sb–V mixed oxides depends on the aspects such as Sb/V ratio, preparation method and thermal treatment [15]. In the XRD patterns of $VSbO_x/SiO_2$ catalysts, no diffraction peak for Sb_2O_4 or Sb_2O_5 can be observed, suggesting that no crystalline antimony oxide with remarkable size exists on $VSbO_x/SiO_2$ catalysts. This is in good agreement with the fact that no diffraction peak of bulk antimony oxides can be observed in the XRD patterns of Sb_2O_5/SiO_2 or Sb_2O_3/SiO_2 catalysts even the loading of Sb_2O_5 or Sb_2O_3 reaches 20 wt% [24,25]. Xie and Tang also found that antimony oxide can disperse spontaneously to the surface and pores of zeolites [27]. Additionally, no diffraction peak for V_2O_5 can be observed in the XRD patterns of $VSbO_x/SiO_2$ catalysts, suggesting that no crystalline V_2O_5 big enough to be detected by XRD has formatted.

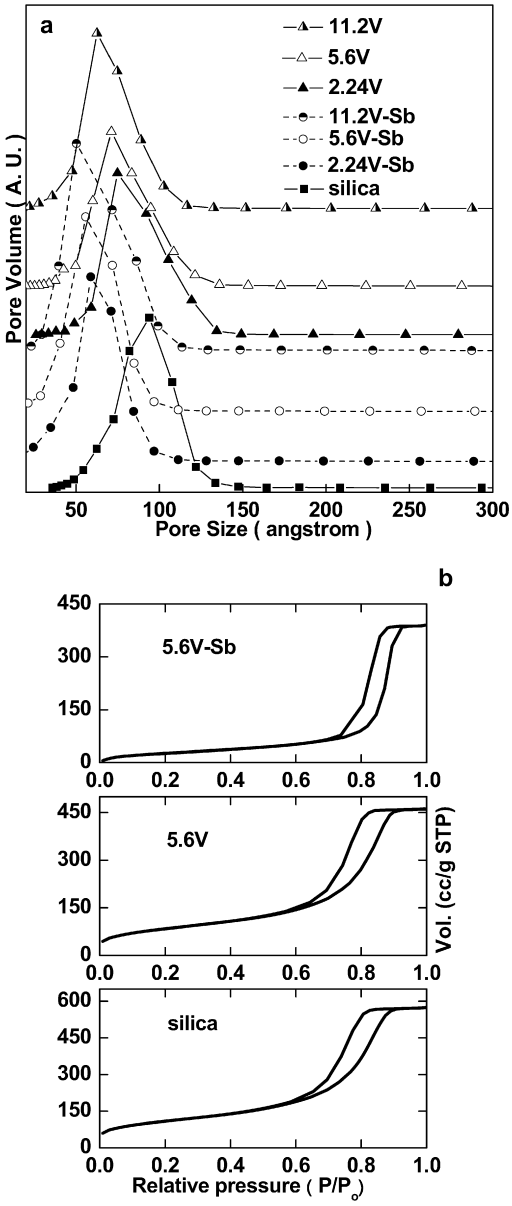

Fig. 1. (a) pore size distribution by desorption branches of N_2 adsorption–desorption isotherms and (b) N_2 adsorption–desorption isotherms of silica support, 5.6V and 5.6V–Sb catalysts.

Table 1
Textural and chemical properties of SiO_2, VO_x/SiO_2 catalysts and $VSbO_x/SiO_2$ catalysts

Catalysts	Pore diameter (nm)	Specific area (m^2/g)	Content of V (wt% V_2O_5)	Content of Sb (wt% Sb_2O_5)	Sb/V ratio
SiO_2	9.3	391	–	–	–
2.24V	7.5	312	2.1	–	–
5.6V	7.0	287	5.4	–	–
11.2V	6.2	255	10.9	–	–
2.24V–Sb	5.2	223	2.2	19.3	5.2
5.6V–Sb	4.8	179	5.3	19.5	2.1
11.2V–Sb	4.5	118	10.4	19.2	1.0

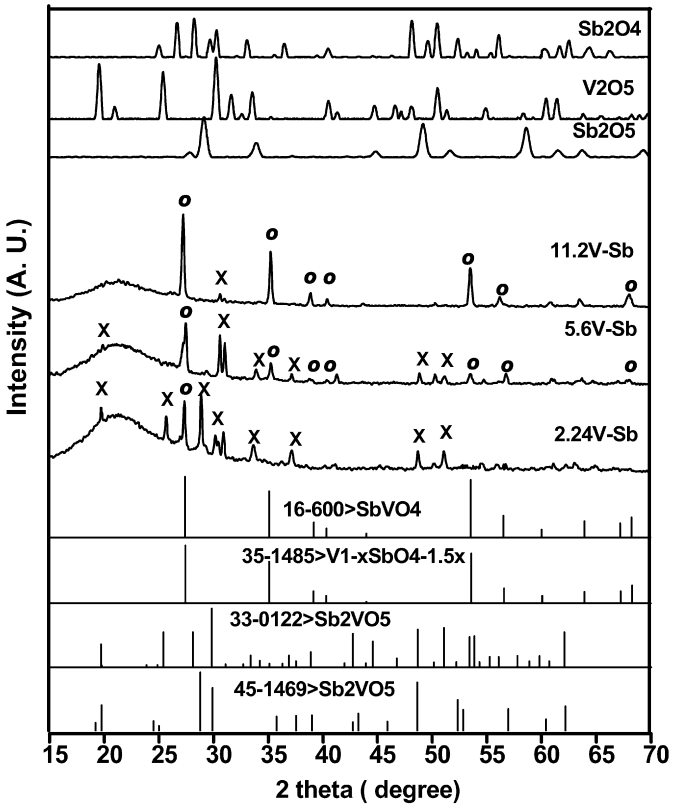

Fig. 2. XRD patterns of $VSbO_x/SiO_2$ catalysts, V_2O_5, Sb_2O_4 and Sb_2O_5 (×, Sb_2VO_5; ○, $SbVO_4/VSb_{1-x}O_{4-1.5x}$).

In the XRD pattern of 2.24V–Sb catalyst, the characteristic peaks of the Sb–V mixed oxide in Sb_2VO_5 phase at 19.2°, 25.4°, 28.1°, 29.8°, 33.4°, 36.9°, 48.7° and 51.1° are predominant. These diffraction peaks become weak when V_2O_5 loading increases to 5.6 wt%. The characteristic peaks of Sb–V mixed oxide in Sb_2VO_5 phase disappear while V_2O_5 loading reaches to 11.2 wt% but only the characteristic peaks of the Sb–V mixed oxide in $SbVO_4/VSb_{1-x}O_{4-1.5x}$ phases at 27.3°, 35°, 39.2°, 40.4°, 53.5°, 56.5° and 68.3° can be observed in the XRD pattern of 11.2V–Sb catalyst. The variation of diffraction peaks with increasing vanadium concentration suggests that the phases of the Sb–V mixed oxides in 5.6V–Sb and 11.2V–Sb catalysts transfer from Sb_2VO_5 phase to $SbVO_4/VSb_{1-x}O_{4-1.5x}$ phase. The XRD results demonstrate the formation of the Sb–V mixed oxide on $VSbO_x/SiO_2$ catalysts and the phase variation of the Sb–V mixed oxide with changing vanadium concentration.

3.2.2. H_2-TPR studies

Fig. 3 gives the H_2-TPR profiles of $VSbO_x/SiO_2$, Sb_2O_5/SiO_2 and VO_x/SiO_2 catalysts. In the TPR profiles of all VO_x/SiO_2 catalysts, the reduction peak at 530 °C can be observed. This TPR peak can be attributed to the reduction of highly isolated tetrahedral V^{5+} and low oligomeric V^{5+} entities, being consistent with the H_2-TPR studies on VO_x/SiO_2 catalysts [28,29] and VO_x/MCM-41 catalysts [10]. Meanwhile, in addition to the peak at 530 °C, a little shoulder at ca. 668 °C was observed in the profile of 11.2V catalyst. This little shoulder should be assigned to the reduction peak of highly aggregated V^{5+} species. Comparing with the H_2-TPR profiles of 20 wt% Sb_2O_5/SiO_2 catalyst and VO_x/SiO_2 catalysts, it is clear that the reduction peaks, observed in the range of 610–720 °C of the H_2-TPR profiles of $VSbO_x/SiO_2$ catalysts, are not related to SbO_x species or VO_x species. This reflects the formation of Sb–V mixed oxide species in the $VSbO_x/SiO_2$ catalysts, being consistent with the XRD results shown in Fig. 2. These reduction peaks of $VSbO_x/SiO_2$ catalysts should be attributed to the reduction of the

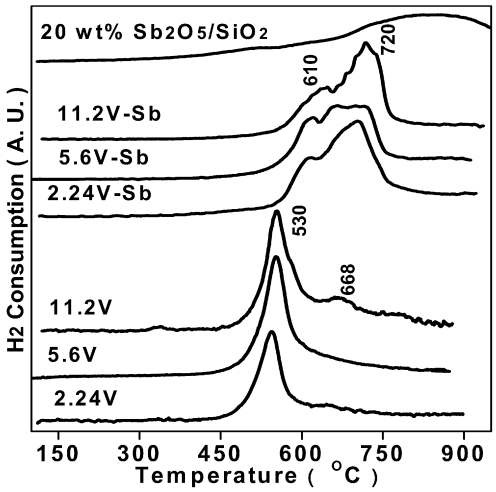

Fig. 3. H_2-TPR profiles of $VSbO_x/SiO_2$, Sb_2O_5/SiO_2 and VO_x/SiO_2 catalysts.

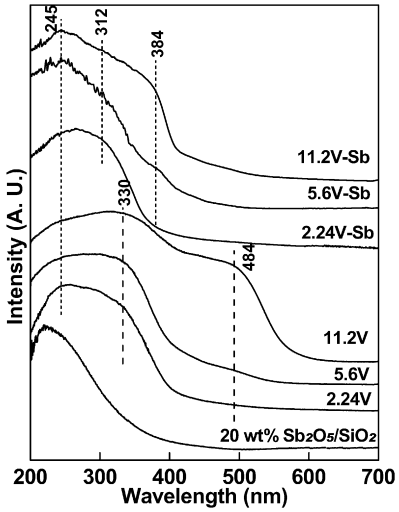

Fig. 4. UV–vis DRS spectra of $VSbO_x/SiO_2$, VO_x/SiO_2 and 20 wt% Sb_2O_5/SiO_2 catalyst.

vanadium containing species in the frameworks of Sb–V mixed oxide because the reduction of SbO_x species needs much higher temperature than 700 °C.

3.2.3. UV–vis DRS studies

Fig. 4 presents the UV–vis DRS spectra of all catalysts after dehydration at 500 °C. Being different from the spectra of 20 wt% Sb_2O_5/SiO_2 catalyst, three absorbance bands centered at 245, 330 and 484 nm can be identified in the spectra of VO_x/SiO_2 catalysts. Baltes et al. [7] assigned the O → V charge transfer (CT) bands at 250 and 354 nm, observed for VO_x/MCM-48 catalysts, to isolated tetrahedral VO_x and tetrahedral chains of VO_x linked to each other by V–O–V bridges. Such assignments of the O → V CT bands, centered at ca. 243–250 nm and 315–320 nm, are also in good agreement with the studies on vanadia catalysts on different supports [10–12,30,31]. Then, the band at 245 nm in the spectrum of 2.24V catalyst should be assigned to highly isolated monomeric VO_x species and another band at 330 nm should be assigned to low oligomeric VO_x species with V–O–V bridges [7,10–12,30,31]. In addition, the VO_x species in 2.24V catalyst should be V^{5+} entities as proposed by Baltes et al. [7], Berndt et al. [10] and Fornes et al. [11].

For 5.6V catalyst, the absorbance bands at 245 and 330 nm can also be observed but an energy decrease of the adsorption edge is identified, reflecting an increase in the size and dimensionality

of VO_x domains. A new broad band at 484 nm emerges in the spectrum of 5.6V catalyst and becomes much more intensive in the spectrum of 11.2V catalyst. The presence of this band at 484 nm in the spectra of 5.6V and 11.2V catalysts can indicate the formation of aggregated VO_x species or even microcrystalline of V_2O_5 [10–12].

$VSbO_x/SiO_2$ catalysts present different spectra, in which three absorbance bands at 245, 312 and 384 nm are identified, from that of 20 wt% Sb_2O_5/SiO_2 catalyst. The attribution of these three bands to V species goes straight. Being similar to the bands at 245 nm in the spectra of VO_x/SiO_2 catalysts, the bands at 245 nm in the spectra of $VSbO_x/SiO_2$ catalysts can be attributed to highly isolated monomeric VO_x species with V=O bands. The intensity of another band at 312 nm increases with increasing loading of V_2O_5, suggesting that this band should be related to oligomeric tetrahedral VO_x species. This is consistent with the reported characteristics of oligomeric tetrahedral VO_x species [7,10–12,30,31].

Considering the Sb/V ratio of $VSbO_x/SiO_2$ catalysts and the absence of the bands at 330 or 484 nm in the spectra of $VSbO_x/SiO_2$ catalysts, the VO_x species in the $VSbO_x/SiO_2$ catalysts should be linked to each other by V–O–Sb bridges. This can explain why the absorbance bands for the oligomeric tetrahedral VO_x species in $VSbO_x/SiO_2$ catalysts are centered not at 330 nm but at 312 nm. The Sb–O–V linkage shows a higher energy absorption edge than the V–O–V linkage. This could be due to the difference in electronegativities of Sb and V. In the spectra of 5.6V–Sb and 11.2V–Sb catalysts, the band at 245 nm becomes much more remarkable than in the spectrum of 2.24V–Sb catalyst, suggesting the possible increase of monomeric VO_x species owing to the presence of antimony species.

The band of highly aggregated vanadia entities, related to the band at 484 nm in the spectra of VO_x/SiO_2 catalysts, cannot be observed in the spectra of all $VSbO_x/SiO_2$ catalysts even the concentration of V_2O_5 reaches 11.2 wt%, indicating no aggregated vanadia entities arises in $VSbO_x/SiO_2$ catalysts. A band at 384 nm arises in the spectrum of 5.6V–Sb catalyst and this band becomes much more intensive in the spectrum of 11.2V–Sb catalyst. This band is centered at the position between the bands for oligomeric tetrahedral VO_x species (or square pyramidal VO_x species) and the bands for aggregated VO_x species (or even microcrystalline of V_2O_5). Then it should be attributed to the oligomeric Sb–O–V species. This attribution is agreed with the fact that the UV–vis DRS bands for $VSbO_x/SiO_2$ catalysts are located in the shorter wavelength zone comparing with the bands for VO_x/SiO_2 catalysts. Because of the existence of Sb–O–V bridges in $VSbO_x/SiO_2$ catalysts, the relative amount of monomeric VO_x species is higher than VO_x/SiO_2 catalysts as reflecting by the intensity of the band at 245 nm in the spectra of $VSbO_x/SiO_2$ catalysts.

3.2.4. UV Raman spectroscopy studies

The UV Raman spectra, given in Fig. 5, provide further information about the species on $VSbO_x/SiO_2$ and VO_x/SiO_2 catalysts. In the Raman spectra of 2.24V–Sb and 5.6V–Sb catalysts, we can see four Raman bands at 190, 260, 400 and 460 cm^{-1} relevant to Sb_2O_4 [24], indicating the formation of microcrystalline of Sb_2O_4 on the surface of $VSbO_x/SiO_2$ catalysts. The mole value of antimony is higher than that of vanadium in 2.24V–Sb (Sb/V = 5.2) and 5.6V–Sb (Sb/V = 2.1) catalysts. Then the presence of antimony oxide species in addition to Sb–V mixed oxide on the catalyst surface is reasonable [20]. However, the antimony oxide species on the surface of $VSbO_x/SiO_2$ catalysts, even with the Sb_2O_5 loading at 20 wt%, cannot to be recognized by XRD because of well dispersion of antimony oxide species [20,24,25]. The decreasing intensity of these four bands, which are related to Sb_2O_4, with increasing V_2O_5 loading may indicate that the amount of Sb_2O_4 species decreases with increasing V_2O_5 loading. Another possibility for the decrease of the intensities of these four bands should be considered. The intensities of these Sb_2O_4 bands may decrease due to self-absorption caused by the addition of vanadium. Comprehensive analysis of the results of XRD, H_2-TPR, UV–vis DRS and UV Raman leads to former one. In the spectrum of 11.2V–Sb (Sb/V = 1) catalyst, no Raman band of Sb_2O_4 can be observed, suggesting that most Sb containing species should exist as Sb–V mixed oxide.

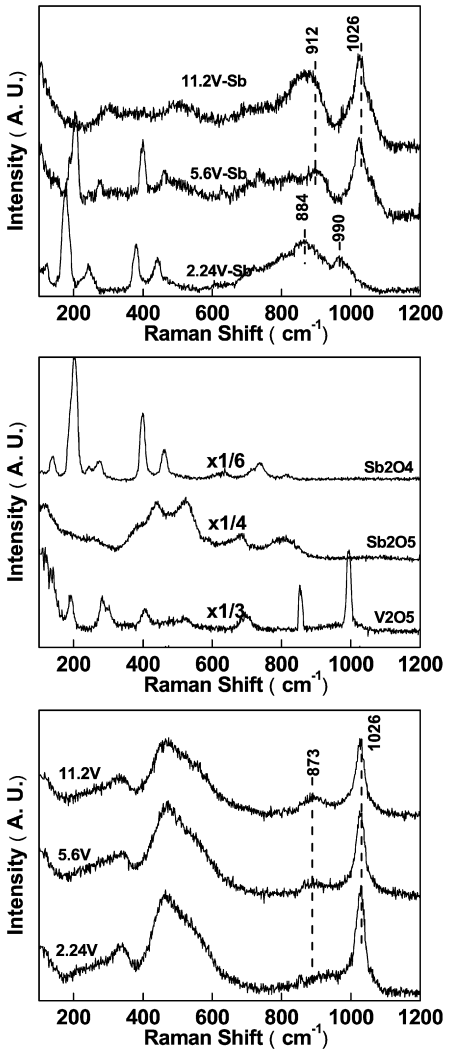

Fig. 5. UV Raman spectra of $VSbO_x/SiO_2$ catalysts, VO_x/SiO_2 catalysts, V_2O_5, Sb_2O_4 and Sb_2O_5. $\lambda_{ex} = 325$ nm.

In the Raman spectra of $VSbO_x/SiO_2$ catalysts, three bands at 884, 912 and 990 cm^{-1} can be identified and attributed to Sb–V mixed oxide according to recent Raman studies on unsupported Sb–V mixed oxide materials [32–35] and supported Sb–V mixed oxide materials [19,20]. The bands at 884 and 912 cm^{-1}, which have not been reported previously, are prominent here due to resonance Raman enhancement from the excitation line at 325 nm [34,36]. The bands at 884 cm^{-1} should be assigned to the Sb–O–V stretching mode of Sb–V mixed oxide. This assignment is in agreement with the shift of such Sb–O–V vibration band from 884 to 912 cm^{-1} in the Raman spectrum of 5.6V–Sb catalyst.

The Raman band centered at 912 cm^{-1} can also be observed in the Raman spectrum of 11.2V–Sb catalyst. It becomes more intensive and broad than that for 5.6V–Sb catalyst. Polymeric $(VO_3)_n$ species present characteristic vibration band centered at 873 cm^{-1} of V–O–V bridge [33,36]. As observed in the Raman spectra of VO_x/SiO_2 catalysts, this band at 873 cm^{-1} is not intensive even the loading of V_2O_5 reaches 20 wt%. In the spectrum of 11.2V–Sb,

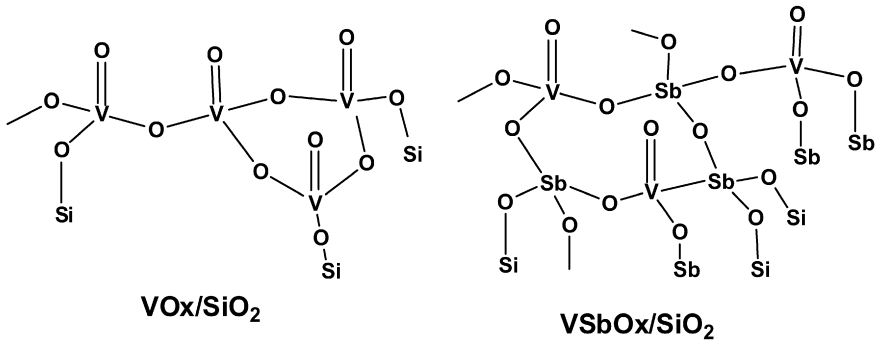

Scheme 1. Schematic illustration of the different motifs of VO_x and $VSbO_x$ species on the surface of VO_x/SiO_2 and $VSbO_x/SiO_2$ catalysts.

the much lower Raman shifts for V–O–V vibrations suggested by the calculations did by Magg et al. [37] are also absent. Then the attribution of this band in the spectra of 11.2V–Sb to the Sb–O–V stretching mode of Sb–V mixed oxide is reasonable. This suggests that more Sb–V mixed oxide with Sb–O–V bridge formed on the surface of 11.2V–Sb catalyst. This tendency is agreed with the UV–vis DRS results shown in Fig. 4. Then an schematic illustration of the different motifs of the structures of VO_x and $VSbO_x$ species on the surfaces of VO_x/SiO_2 and $VSbO_x/SiO_2$ catalysts can be proposed as shown in Scheme 1.

In the spectrum of 2.24V–Sb catalyst, a Raman band at 990 cm^{-1} can be observed. The UV Raman spectrum of crystalline V_2O_5 also shows a characteristic band at 990 cm^{-1}, which is assigned to the V=O stretching vibration mode of bulk V_2O_5, as shown in Fig. 5. Xiong et al. studied unsupported $VSbO_x$ samples (Sb/V = 1) by UV Raman and XRD [34]. They attributed the peak at 990 cm^{-1} to the V=O stretching vibration mode of crystalline V_2O_5 since the XRD data indicate that both V_2O_5 and Sb_2O_4 are present and the peaks from these phases must be considered. Their samples were prepared from V_2O_5 and Sb_2O_3 and thus the residual of bulk V_2O_5 in such final $VSbO_x$ samples is reasonable or even inevitable. In the present work, the $VSbO_x$ phase of 2.24V–Sb catalyst (Sb/V = 5) was prepared from $SbCl_5$ and NH_4VO_3 and dispersed on high specific area silica. Although the absence of diffraction peak for V_2O_5 in the XRD patterns of $VSbO_x/SiO_2$ catalysts may results from the very small amount of V_2O_5 with very small size, the formation of crystalline V_2O_5 is not predominant. On the contrary, the XRD peaks of Sb–V mixed oxide are clear. In addition, the Raman peak at 873 cm^{-1} of V–O–V bridge [33,36] is absent in the spectrum of 2.24V–Sb catalyst. Thus the band at 990 cm^{-1} in the spectrum of 2.24V–Sb catalyst should be assigned to the V=O stretching vibration mode of Sb–V mixed oxide [19,20].

In the Raman spectra of 5.6V–Sb and 11.2V–Sb catalysts, the band of V=O stretching vibration mode becomes broad and shifts to 1026 cm^{-1}, suggesting that more Sb–V mixed oxide domains formed and more V=O site exposed on the surfaces of these two catalysts because UV Raman is a surface sensitive technology. This is also suggested by the increasing intensity of the bands, which are centered at 245 nm in the UV–vis spectra of $VSbO_x/SiO_2$ catalysts (Fig. 4), with increasing loading of V_2O_5. Oligomeric tetrahedral VO_x species (or square pyramidal VO_x species) with Sb–O–V bridge emerges in 5.6V–Sb catalyst and become considerably rich in 11.2V–Sb catalyst. In the Raman spectra of VO_x/SiO_2 catalysts, the bands at 1026 and 873 cm^{-1}, which are relevant to monomeric VO_x species and polymeric $(VO_3)_n$ species, can be observed as well as the bands at ca. 460 cm^{-1} for amorphous silica. We can see that the amount of aggregated VO_x species in VO_x/SiO_2 catalysts significantly increases with increasing V_2O_5 loading according to the intensity of the bands at 873 and 1026 cm^{-1} (Fig. 5). In line with the UV–vis DRS results (Fig. 4), we can know that the amount of aggregated VO_x species in VO_x/SiO_2 catalysts is remarkably higher than that in $VSbO_x/SiO_2$ catalysts.

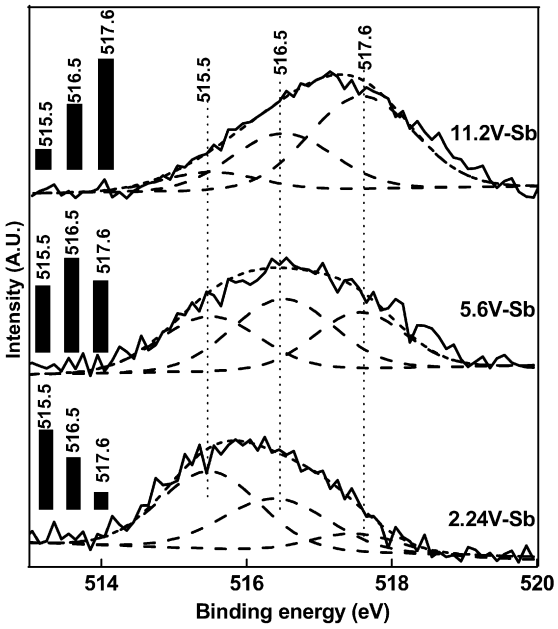

Fig. 6. V $2p_{3/2}$ XPS spectra (solid lines) of $VSbO_x/SiO_2$ catalysts and their fitting curves (dashed lines). The inset black columns demonstrate the contribution of each fitting curve to the sum (short dashed lines) approximating the original V $2p_{3/2}$ peaks.

3.2.5. Oxidation state of V in $VSbO_x/SiO_2$ catalysts

Zanthoff et al. found that, in Sb–V mixed oxide, the average oxidation state of vanadium increases from tetravalent/trivalent to pentavalent with decreasing Sb content [38]. Fig. 6 exhibits the V $2p_{3/2}$ XPS spectra of $VSbO_x/SiO_2$ catalysts. We can see that the maximum of V $2p_{3/2}$ peak shifts to higher binding energy from 516.0 eV to 517.2 eV with decreasing Sb/V ratio. It can be proposed that the average oxidation state of V in $VSbO_x/SiO_2$ catalysts increases with decreasing Sb/V ratio. All these three V $2p_{3/2}$ peaks can be well fitted by three Gaussian curves with maxima at 515.5, 516.5 and 517.6 eV, which are relevant to V^{3+}, V^{4+} and V^{5+} entities, respectively [38–40]. The inset black columns in Fig. 6 demonstrate the contribution of each fitting curve to the sum approximating the original V $2p_{3/2}$ peaks. It is clear that V^{5+} entity is predominant in 11.2 V–Sb catalyst while V^{3+} entity is little in this catalyst. On the contrary, 2.24 V–Sb catalyst exhibits an opposite trend for the contribution of vanadium entities. In 5.6 V–Sb catalyst, V^{4+} entity is predominant while the concentration of V^{5+} or V^{3+} entities is lower and on almost same level.

3.2.6. Surface acidity of $VSbO_x/SiO_2$ and VO_x/SiO_2 catalysts

Fig. 7 comparatively presents the FT-IR spectra of 5.6V–Sb and 5.6V catalysts after the adsorption of pyridine and subsequent

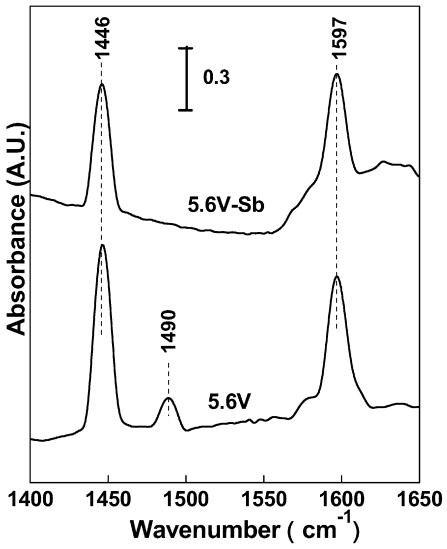

Fig. 7. FT-IR spectra of the pyridine adsorbed on 5.6V–Sb and 5.6V catalysts evacuated at 150 °C.

Table 2
Catalytic performance for $VSbO_x/SiO_2$ and VO_x/SiO_2 catalysts in methanol selective oxidation.

Catalysts	T (°C)	CH_3OH conv. (%)	Product contribution (%)			
			HCHO	CO_x	DME	Other oxygenates
2.24V–Sb	400	65.8	85.0	15.0	Trace	n.d.[a]
	438	94.5	79.4	20.0	Trace	Trace
5.6V–Sb	400	85.8	86.4	6.0	5.0	0.5
	425	99.6	91.0	6.2	2.0	0.8
11.2V–Sb	400	92.4	70.8	9.6	18.0	1.2
2.24V	400	73.6	74.1	21.5	3.0	1.0
	425	99.7	68.3	29.6	1.0	1.0
5.6V	400	99.1	68.9	22.9	6.1	2.1
	425	99.6	52.0	38.0	0	n.d.
11.2V	400	99.1	62.5	29.3	8.2	n.d.

[a] n.d.: not detected.

evacuation at 150 °C. In the spectra of 5.6V catalyst, three IR bands centered at 1446, 1490, 1597 cm^{-1} can be observed. The band at 1490 cm^{-1} can be attributed to the interaction of the pyridine adsorbed on Lewis and Brönsted acid sites [41,42]. This band at 1490 cm^{-1} cannot be observed in the spectrum of 5.6V–Sb catalyst. Another band at 1446 cm^{-1} can be assigned to the pyridine coordinatively bonded to the defect sites of distorted silica network as weak Lewis acidic sites [42] or to hydrogen-bonded pyridine [43]. Some other researchers also assigned the bands at 1446 and 1597 cm^{-1} to the physisorbed pyridine [41]. Nevertheless, we know that 5.6V–Sb catalyst presents lower acidity than 5.6V catalyst because of the absence of the IR band at 1490 cm^{-1} in the spectrum of 5.6V–Sb catalyst. The studies on other $VSbO_x/SiO_2$ and VO_x/SiO_2 catalysts give same trend of surface acidity as that explicated by the studies on 5.6V–Sb and 5.6V catalysts. The introduction of Sb into vanadia catalysts can reduce the surface acidity of catalysts [18] and thus provides a possibility to adjust the surface acidity by changing the Sb/V ratio of $VSbO_x/SiO_2$ catalysts.

3.3. Selective oxidation of methanol

Table 2 shows the reaction results of $VSbO_x/SiO_2$ and VO_x/SiO_2 catalysts in methanol selective oxidation using O_2 as oxidant. At 400 °C, all $VSbO_x/SiO_2$ catalysts exhibit relatively lower methanol conversion but higher formaldehyde selectivity than that for corresponding VO_x/SiO_2 catalysts with same V_2O_5 loading. Notably, the CO_x selectivity for $VSbO_x/SiO_2$ catalysts, in particularly for either 5.6V–Sb catalyst or 11.2V–Sb catalyst, is much lower than that for corresponding VO_x/SiO_2 catalysts. According to the data listed in Table 2, we can compare the catalytic performance for $VSbO_x/SiO_2$ and VO_x/SiO_2 catalysts at similar methanol conversions near to 100%. For 2.24V–Sb and 5.6V–Sb catalysts, the methanol conversions increase to 100% with increasing reaction temperature while the corresponding formaldehyde selectivity drops slightly (for 2.24V–Sb) or even increases softly (5.6V–Sb). At 425 °C, the formaldehyde selectivity up to 91.0% with a methanol conversion at 99.6% can be obtained for 5.6V–Sb catalyst while corresponding 5.6V catalyst produces less formaldehyde (62.0% formaldehyde selectivity) but more CO_x (38.0% CO_x selectivity).

Furthermore, we can see that the main products for 2.24V–Sb and 5.6V–Sb catalysts are formaldehyde and CO_x with trace amount of DME but a certain amount of DME can be produced on 11.2V–Sb catalyst. The selectivity to DME for $VSbO_x/SiO_2$ catalysts increases evidently with decreasing Sb/V ratio. Being different to $VSbO_x/SiO_2$ catalysts, VO_x/SiO_2 catalysts mainly produce formaldehyde and CO_x with little DME at either 400 or 425 °C. At 400 °C, the selectivity to DME for VO_x/SiO_2 catalysts is higher than that for $VSbO_x/SiO_2$ catalysts and also increases with increasing loading of V_2O_5. Generally, the CO_x selectivity for VO_x/SiO_2 catalysts is much higher (even more than 6 times higher for 5.6V catalyst comparing with 5.6V–Sb catalyst at 425 °C) than that for $VSbO_x/SiO_2$ catalysts. $VSbO_x/SiO_2$ catalysts, especially 5.6V–Sb, are highly active and much more selective in methanol selective oxidation than VO_x/SiO_2 catalysts.

Fig. 8 shows the catalytic performance for 5.6V–Sb and 5.6V catalysts at the temperatures from 350 °C to 425 °C. The methanol conversion, for either 5.6V–Sb or 5.6V catalysts, increases with increasing reaction temperature. The formaldehyde selectivity for 5.6V catalyst drops while the formaldehyde selectivity for 5.6V–Sb catalyst softly increases with increasing reaction temperature. The CO_x selectivity for 5.6V–Sb catalyst is significantly lower than that for 5.6V catalyst at each temperature, indicating that the deep oxidation of intermediates and products is effectively suppressed on 5.6V–Sb catalyst. The DME selectivity for 5.6V–Sb catalyst is lower than that for 5.6V catalyst at each temperature. Fig. 9 exhibits the catalytic performance of 5.6V–Sb catalyst in a 14 h run. One-pass yield of formaldehyde more than 90% with the production of CO_x less than 7% can be obtained and well kept in the test for 14 h. This reflects that the structure of the active sites in 5.6V–Sb catalyst is stable or the leaching of active component is imperceptible under reaction conditions, in which the reaction temperature is much lower than the calcination temperature (700 °C) for the catalyst.

From Fig. 6, we can know that the average oxidation state of vanadium for $VSbO_x/SiO_2$ catalyst increases with decreasing Sb/V ratio. Vanadium species with higher valence state are generally relevant to higher activity. Rybarczyk et al. reported that, in the oxidative dehydrogenation of propane, V^{4+} entities seem to be more selective, although less active, than V^{5+} entities, due to its lower oxidation potential [44]. Then it is not surprising to see that the activity for $VSbO_x/SiO_2$ catalyst increases with decreasing Sb/V ratio and 5.6V–Sb catalyst shows both high methanol conversion and high formaldehyde selectivity. From the results of UV–vis DRS (Fig. 4) and UV Raman (Fig. 5) studies, we know that the relative amount of monomeric VO_x species in $VSbO_x/SiO_2$ catalyst is higher than VO_x/SiO_2 catalysts and the amount of aggregated VO_x species in VO_x/SiO_2 catalysts is significantly higher than that in $VSbO_x/SiO_2$ catalysts. This can explain the lower production of CO_x on $VSbO_x/SiO_2$ catalysts than VO_x/SiO_2 catalysts and the remarkable increase of CO_x selectivity for VO_x/SiO_2 catalysts with increasing loading of V_2O_5. In Table 2, we can see that 2.24V catalyst exhibits a CO_x selectivity higher than 20%. Two points are relevant to such CO_x production. The first one is that

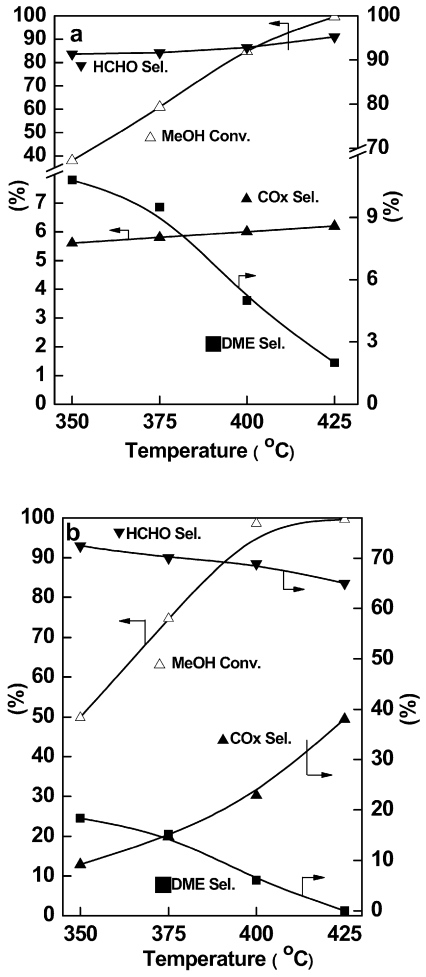

Fig. 8. Catalytic performance for (a) 5.6V–Sb and (b) 5.6V catalysts in methanol selective oxidation.

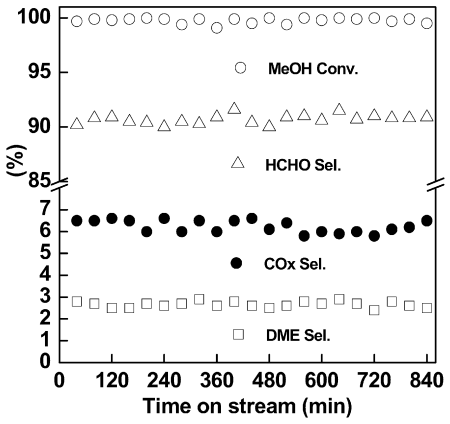

Fig. 9. Catalytic performance for 5.6V–Sb catalyst at 425 °C in methanol selective oxidation. (GC analysis began after 40 min long balance of the reaction.)

the UV–vis DRS spectrum of 2.24V catalyst presents an intensive band at 330 nm, which reflecting the formation of quiet a few low oligomeric VO_x species with V–O–V bridges. In addition, as proposed by some researchers [7,10,11], the VO_x species in 2.24V catalyst should be V^{5+} entities, which is highly activity but less selective.

The production distribution of methanol selective oxidation greatly depends on the acidic and basic properties of the catalysts and the production of formaldehyde needs bi-functional catalysts with acid–base character [14,21]. Strong Lewis acidity of catalysts promotes the production of DME via a dehydration process of methanol [21,22] while distinct basic character leads to CO_x [23]. Liu et al. [12] and Berndt et al. [10] found that the number of both Lewis and Brönsted acid sites increases with vanadia loading on VO_x/SBA-15 and VO_x/MCM-41 catalysts, respectively. The introduction of Sb into vanadia catalysts can reduce the surface acidity of catalysts [18]. The FT-IR spectra of adsorbed pyridine show difference between $VSbO_x/SiO_2$ and VO_x/SiO_2 catalysts but cannot present us a quantitative amount/strength relationship with different V loadings in $VSbO_x/SiO_2$ catalysts. Since the content of antimony in $VSbO_x/SiO_2$ catalysts is constant, it is helpful to delineate the surface acidity of $VSbO_x/SiO_2$ catalysts in following sequence: 2.24V–Sb < 5.6V–Sb < 11.2V–Sb. Consistent with this change of surface acidity, the product contribution of $VSbO_x/SiO_2$ catalysts transforms from a basic character (for 2.24V–Sb catalyst) to an acid character (for 11.2V–Sb catalyst) via an acid–base character (for 5.6V–Sb catalyst) as shown in Table 2.

5.6V–Sb catalyst presents lower surface acidity than 5.6V catalysts as reflected by Fig. 7. Then it is not surprising to see that higher selectivity to DME can be obtained on 5.6V catalyst than 5.6V–Sb catalyst as shown in Fig. 8. In addition, the desorption of formaldehyde can also be favored on 5.6V–Sb catalyst, which shows mild acidity, and then the depression of overoxidation can thus be favored. However, although the surface acidity of 5.6V catalyst is higher than that of 5.6V–Sb catalyst and the DME selectivity for 5.6V catalyst is also higher than that for 5.6V–Sb catalyst, the main by-product for 5.6V catalyst is not DME but CO_x. In Fig. 8 we can see that the CO_x selectivity for 5.6V catalyst is much higher than that for 5.6V–Sb catalyst and increases rapidly with increasing temperature. On the contrary, the selective formation of formaldehyde is favored on 5.6V–Sb catalyst while the formation of CO_x is depressed. For 5.6V–Sb catalyst, formaldehyde selectivity increases softly with increasing temperature while the selectivity to DME exhibits a drop with increasing temperature. This because the desorption rate of formaldehyde is enhanced more by a temperature increase than is the reaction rate to form dioxymethylene species [23].

3.4. *In situ* DRIFTS studies on the methanol selective oxidation on 5.6V and 5.6V–Sb catalysts

The first step of the methanol selective oxidation on supported vanadium oxide is the chemisorption of methanol to the surface VO_x species with the formation of methoxy species [4,8,21,45]. In second step, the C–H bonds in the adsorbed methoxy groups are broken and formaldehyde is released. Here, *in situ* DRIFTS was employed to comparatively study the methanol selective oxidation on 5.6V and 5.6V–Sb catalysts.

Fig. 10 gives the *in situ* DRIFTS spectra of the species arising from the methanol selective oxidation on 5.6V catalysts. In Fig. 10a, a characteristic band of isolated Si–OH groups at 3740 cm^{-1} is clear in the spectrum acquired 30 s later after the chamber was heated to 350 °C. Because the spectrum was collected by the subtraction of pretreated reference sample for making the bands of adsorbed species more clear, the silanol OH band appears as a negative one. Thus the decreasing intensity of this band with time on stream indicates an increase in its concentration. This band at 3740 cm^{-1} disappears after 360 s, suggesting no adsorbed species linked to Si–OH groups after 360 s. Fig. 10b presents the C–H stretching region, in which the bands at 2859, 2936, 2959 and 2995 cm^{-1} are observed. These bands are characteristic of the C–H vibration modes of methoxy groups (CH_3O–) formed by the adsorption of methanol on catalyst surface [45–48]. The intensity of these bands for methoxy groups decreases with time on stream. Correspondingly, in Fig. 10c, we can see the characteristic bands

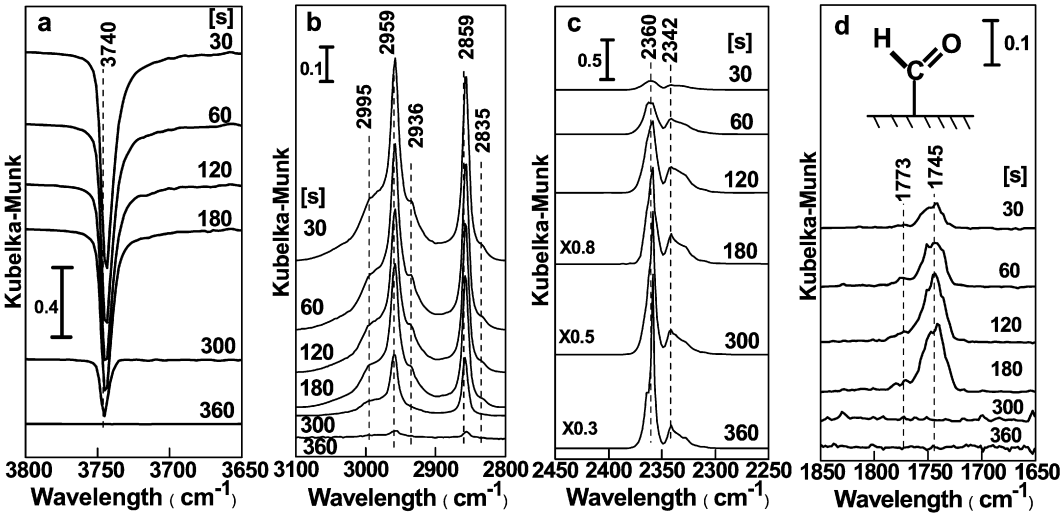

Fig. 10. *In situ* DRIFTS spectra of the species formed in the methanol selective oxidation on 5.6V catalyst in the mixture of O_2 and N_2; time from the beginning of reaction is indicated.

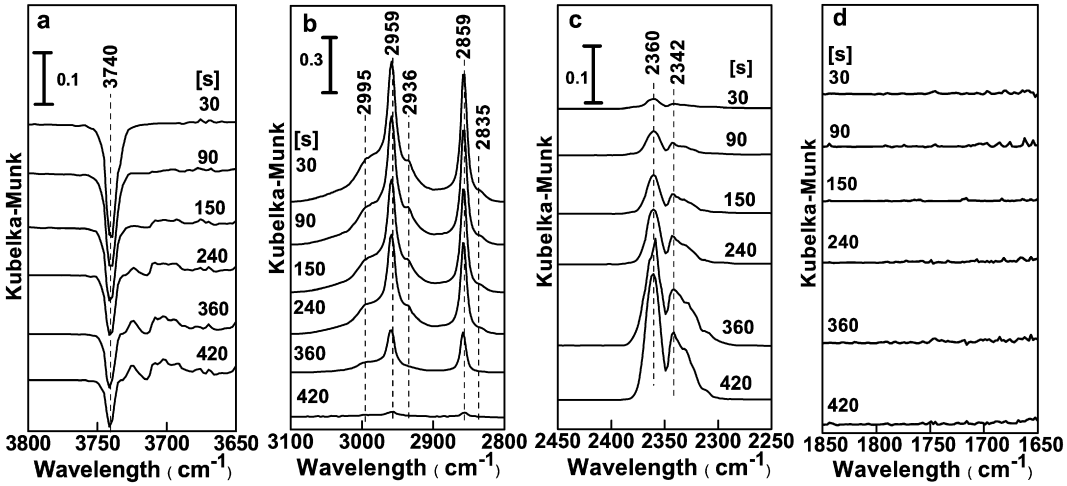

Fig. 11. *In situ* DRIFTS spectra of the species formed in the methanol selective oxidation on 5.6V–Sb catalyst in the mixture of O_2 and N_2; time from the beginning of reaction is indicated.

for gaseous CO_x at 2342 and 2360 cm^{-1} become much intensive with time on stream, indicating the oxidation of methoxy groups.

Seman et al. [45,46] found that, on MoO_x/SiO_2 catalysts, the support (silica) acts as a storage place for both active and spectator reaction intermediates. The methoxide species (80% in the whole) [46] on the silica support is about 6 times more than that on Mo centers and can migrate to the Mo centers to be oxidized in He/O_2 flow to formaldehyde. Meanwhile, the remaining methoxide species (20%) are inert spectators and can form stable acyl species, which are considered as a dead end in the oxidation process, producing CO_x and H_2O [46]. During the oxidation of methoxy groups, two bands at 1745 and 1773 cm^{-1} are observed as shown in Fig. 10d. These two bands are characteristically assigned to the C=O stretching modes of adsorbed acyl species according to recent studies of methanol oxidation on MoO_x/SiO_2 catalysts [45,46]. As Seman et al. suggested, this acyl species was found not to be involved in selective reaction sequence but to produce CO_x and H_2O [46]. Then we can see that the C=O bands become more intensive with time on stream at first but disappear after 300 s, indicating an oxidation sequence, methanol → adsorbed methoxy species → acyl species → CO_x.

Fig. 11 exhibits the *in situ* DRIFTS spectra of the species arising from the methanol selective oxidation on 5.6V–Sb catalysts. The bands of adsorbed methoxy groups (Fig. 11b) and gaseous CO_x (Fig. 11c) can be observed as that for 5.6V catalyst. The bands for adsorbed methoxy groups also become weak while the bands for gaseous CO_x become much intensive with time on stream, indicating the oxidation of methoxy groups to produce CO_x as on 5.6V–Sb catalyst. The intensity of the gaseous CO_x bands for 5.6V catalyst (Fig. 10c) is much intensive than that for 5.6V–Sb catalyst (Fig. 11c), indicating much CO_x is produced on 5.6V catalyst than 5.6V–Sb catalyst. This result is in good agreement with the higher CO_x selectivity for VO_x/SiO_2 catalysts than $VSbO_x/SiO_2$ catalysts as shown in Table 2.

Adsorbed methoxy species on 5.6V–Sb catalyst is oxidized in the flow of N_2-O_2 but the methoxy bands can still be observed after 420 s as shown in Fig. 11b. Correspondingly, in Fig. 11a, we can see that the silanol OH band at 3740 cm^{-1} becomes weak with time on stream but still can be observed after 420 s. This can be explained by the relatively lower activity of 5.6V–Sb catalyst than 5.6V catalyst. The C=O bands of adsorbed acyl species are absence in the C=O vibration modes region presented in Fig. 11d. This indicates that such kind of adsorbed acyl species cannot stably formed on the surface of 5.6V–Sb catalyst. The existence of the adsorbed acyl species on 5.6V catalyst and its absence on 5.6V–Sb catalyst can explain the much lower CO_x selectivity but

much higher formaldehyde selectivity obtained for 5.6V–Sb catalyst than that for 5.6V catalyst in methanol selective oxidation. $VSbO_x/SiO_2$ catalysts, particularly 5.6V–Sb catalyst, are highly selective for formaldehyde because the production of CO_x can be depressed on $VSbO_x/SiO_2$ catalysts. From the studies of XRD, UV–vis DRS, UV Raman, XPS, FT-IR and *in situ* DRIFTS on $VSbO_x/SiO_2$ and VO_x/SiO_2 catalysts, we can know that this advantage in the depression of CO_x production should grow out of the formation of Sb–V mixed oxide on $VSbO_x/SiO_2$ catalysts.

4. Conclusions

Silica supported Sb–V mixed oxide catalysts and vanadia catalysts have been prepared and evaluated in methanol selective oxidation with O_2 as oxidant. The active phase of $VSbO_x/SiO_2$ catalysts is Sb–V mixed oxide, in which the framework of VO_x species is interrupted by the incorporation of Sb atoms so isolated tetrahedrally coordinated VO_x species can be stabilized in the framework of Sb–V mixed oxide. The relative amount of monomeric VO_x species in $VSbO_x/SiO_2$ catalysts is higher than VO_x/SiO_2 catalysts. These supported Sb–V mixed oxide catalysts are stable under the reaction conditions of methanol selective oxidation and thus can exhibit stable catalytic performance. The CO_x selectivity obtained on $VSbO_x/SiO_2$ catalysts is low because the formation of the adsorbed acyl species, which leads to CO_x, is not favored on $VSbO_x/SiO_2$ catalysts. The selectivity to formaldehyde at 99.6% with methanol conversion at 91% can be achieved on 5.6V–Sb catalyst. The catalytic performance of 5.6V–Sb catalyst did not exhibit obvious change after a reaction test for 14 h.

The average oxidation state of the vanadium in $VSbO_x/SiO_2$ catalysts increases with decreasing Sb/V ratio from 5.2 to 1.0. Higher average oxidation state of the vanadium in $VSbO_x/SiO_2$ catalysts is suggested to be relevant to higher activity in methanol selective oxidation band V^{4+} species are more selective to formaldehyde. Meanwhile, the formation of Sb–V mixed oxide on $VSbO_x/SiO_2$ catalysts provides a possibility to adjust the production distribution in methanol selective oxidation by changing Sb/V ratio.

Acknowledgments

The financial supports from the National Basic Research Program of China (Grant No. 2003CB615806 & 2005CB221407) and the National Natural Science Foundation of China (NSFC 20673115, 20773118) are acknowledged.

References

[1] H.R. Gerberich, G.C. Seaman, Formaldehyde, in: Kirk–Othmer Encyclopedia of Chemical Technology, fourth ed., Wiley, New York, 1994, p. 929.
[2] S. Lim, G.L. Haller, Appl. Catal. A 188 (1999) 277.
[3] T. Kim, I.E. Wachs, J. Catal. 255 (2008) 197.
[4] B.M. Weckhuysen, D.E. Keller, Catal. Today 78 (2003) 25.
[5] C. Hess, I. Drake, J.D. Hoefelmeyer, T.D. Tilley, A.T. Bell, Catal. Lett. 105 (2005) 1.
[6] G.S. Wong, D.D. Kragten, J.M. Vohs, J. Phys. Chem. B 105 (2001) 1366.
[7] M. Baltes, K. Cassiers, P. Van Der Voort, B.M. Weckhuysen, R.A. Schoonheydt, E.F.J. Vansant, J. Catal. 197 (2001) 160.
[8] R.Z. Khaliullin, A.T. Bell, J. Phys. Chem. B 106 (2002) 7832.
[9] H.R. Aghabozorg, W.R. Flavell, B.H. Sakakini, J. Catal. 167 (1997) 164.
[10] H. Berndt, A. Martin, A. Brückner, E. Schreier, D. Müller, H. Kosslick, G.U. Wolf, B. Lücke, J. Catal. 91 (2000) 384.
[11] V. Fornes, C. Lopez, H.H. Lopez, A. Martínez, Appl. Catal. A 249 (2003) 345.
[12] Y.M. Liu, Y. Cao, N. Yi, W.L. Feng, W.L. Dai, S.R. Yan, H.Y. He, K.N. Fan, J. Catal. 224 (2004) 417.
[13] B. Ramachandra, J.S. Choi, K.Y. Choo, J.S. Sung, S.D. Song, T.H. Kim, Catal. Lett. 105 (2005) 23.
[14] C.T. Wang, S.H. Ro, Appl. Catal. A 285 (2005) 196.
[15] G. Centi, S. Perathoner, F. Trifirò, Appl. Catal. A 157 (1997) 143.
[16] M.O.G. Pérez, J.L.G. Fierro, M.A. Vicente, M.A. Bañares, J. Catal. 206 (2002) 339.
[17] E.V. Benvenutti, Y. Gaushikem, J. Braz. Chem. Soc. 9 (1998) 469.
[18] J. Spengler, F. Anderle, E. Bosch, R.K. Grasselli, B. Pillep, P. Behrens, O.B. Lapina, A.A. Shubin, H.J. Eberle, H. Knözinger, J. Phys. Chem. B 105 (2001) 10771.
[19] H.D. Zhang, L. Zhang, Z.C. Feng, S.G. Wang, K.Q. Sun, P.L. Ying, C. Li, Chin. J. Catal. 26 (2005) 542.
[20] H.D. Zhang, J. Zhang, K.Q. Sun, Z.C. Feng, P.L. Ying, C. Li, Catal. Lett. 106 (2006) 89.
[21] X. Wang, I.E. Wachs, Catal. Today 96 (2004) 211.
[22] H. Hu, I.E. Wachs, J. Phys. Chem. 99 (1995) 10911.
[23] J.M. Tatibouët, Appl. Catal. A 148 (1997) 213.
[24] H.D. Zhang, K.Q. Sun, Z.C. Feng, P.L. Ying, C. Li, Appl. Catal. A 305 (2006) 110.
[25] H.D. Zhang, P.L. Ying, J. Zhang, C.H. Liang, Z.C. Feng, C. Li, Stud. Surf. Sci. Catal. 147 (2004) 547.
[26] K.S.W. Sing, D.H. Everett, R.A.W. Haul, L. Moscou, R.A. Pierotti, J. Rouquerol, T. Siemieniewska, Pure Appl. Chem. 57 (1985) 603.
[27] Y.C. Xie, Y.Q. Tang, Adv. Catal. 37 (1990) 1.
[28] M.M. Koranne, J.G. Goodwin, B.K. Hodnett, Catal. Today 46 (1998) 127.
[29] F. Arena, N. Giordano, A.J. Parmaliana, J. Catal. 167 (1997) 66.
[30] M. Morey, A. Davidson, H. Eckert, G. Stucky, Chem. Mater. 8 (1996) 486.
[31] M.M. Schraml, A. Wokaun, M. Pohl, H.L. Krauss, Chem. Soc. Faraday Trans. 87 (1991) 2635.
[32] M.O.G. Pérez, J.L. Fierro, M.A. Vicente, M.A. Bañares, J. Catal. 206 (2002) 339.
[33] M.A. Bañares, I.E. Wachs, J. Raman. Spectrosc. 33 (2002) 359.
[34] G. Xiong, V.S. Sullivan, P.C. Stair, G.W. Zajac, S.S. Trail, J.A. Kaduk, J.T. Golab, J.F. Brazdil, J. Catal. 230 (2005) 326.
[35] M.O.G. Pérez, M.A. Bañares, Chem. Commun. (2002) 1292.
[36] C. Li, J. Catal. 216 (2003) 203.
[37] N. Magg, B. Immaraporn, J.B. Giorgi, T. Schroeder, M. Bäumer, J. Döbler, Z.L. Wu, E. Kondratenko, M. Cherian, M. Baerns, P.C. Stair, J. Sauer, H.J. Freund, J. Catal. 226 (2004) 88.
[38] H.W. Zanthoff, W. Grünert, S. Buchholz, M. Heber, L. Steievano, F.E. Wagner, G.U. Wolf, J. Mol. Catal. A 162 (2000) 443.
[39] D.W. Park, B.K. Park, D.K. Park, H.C. Woo, Appl. Catal. A 223 (2002) 215.
[40] C. Hess, J. Catal. 248 (2007) 120.
[41] O.M. Busch, W. Brijoux, S. Thomson, F. Schüth, J. Catal. 222 (2004) 174.
[42] H. Kosslick, G. Lischke, G. Walther, W. Storek, A. Martin, R. Fricke, Microporous Mater. 9 (1997) 13.
[43] E.P. Parry, J. Catal. 2 (1963) 371.
[44] P. Rybarczyk, H. Berndt, J. Radnik, M.-M. Pohl, O. Buyevskaya, M. Baerns, A. Brückner, J. Catal. 202 (2001) 45.
[45] M. Seman, J.N. Kondo, K. Domen, R. Radhakrishnan, S.T. Oyama, J. Phys. Chem. B 106 (2002) 12965.
[46] M. Seman, J.N. Kondo, K. Domen, C. Reed, S.T. Oyama, J. Phys. Chem. B 108 (2004) 3231.
[47] A.G. Pelmenschikov, G. Morosi, A. Gamba, A. Zecchina, S. Bordiga, E.A. Paukshtis, J. Phys. Chem. 97 (1993) 11979.
[48] L.J. Burcham, M. Badlani, I.E. Wacha, J. Catal. 203 (2001) 104.